JOURNAL OF PROPULSION AND POWER
Vol. 14, No. 6, November–December 1998

Wall Pressure Measurements for a Sonic Jet Injected Transversely into a Supersonic Crossflow

D. E. Everett*
Whirlpool Corporation, St. Joseph, Michigan 49085
M. A. Woodmansee† and J. C. Dutton‡
University of Illinois at Urbana–Champaign, Urbana, Illinois 61801
and
M. J. Morris§
Bradley University, Peoria, Illinois 61625

The pressure-sensitive-paint technique was used to determine the continuous surface-pressure field around a sonic jet injected transversely into a supersonic freestream of Mach 1.6. Three experimental conditions, with jet-to-crossflow momentum flux ratios of approximately 1.2, 1.7, and 2.2, were examined. The maximum static pressure upstream of the jet injection site was observed to increase with increasing momentum flux ratio, as did the size and streamwise extent of the low-pressure region downstream of the injector. About the circumference of the orifice, the pressure was observed to increase with increasing momentum flux ratio at the upstream edge of the jet, but was essentially independent of this ratio about the rest of the injector periphery. As a result of these pressure measurements, the effective back pressure, which is defined here as the circumferentially averaged wall pressure about the orifice periphery, was observed to increase weakly with increasing jet-to-crossflow momentum flux ratio over the range investigated.

Introduction

THE flowfield resulting from a gaseous jet injected transversely into a supersonic freestream has been studied for quite some time. Early emphasis was directed toward aerodynamic control of supersonic vehicles at high altitude. Schlieren and shadowgraph photographs provided qualitative information about the structure of the resulting flowfield. This flowfield is illustrated in Fig. 1. As the jet is injected into the primary flow, it acts as an obstacle about which the crossflow must move. This obstruction results in the formation of a bow shock in the primary flow upstream of the injector port. A separation shock (the leading leg of the lambda shock) is also generated. The resulting shock-boundary-layer interaction causes a complex pressure field to be established in the near-jet region. For underexpanded jet conditions, after expanding at the injector exit, the jet fluid eventually compresses through a barrel shock or through a Mach disk to equalize the jet pressure with the surrounding freestream pressure. The portion of the jet that passes through the Mach disk loses much of its momentum and is turned downstream by the momentum of the freestream.

Initial experimental studies of the transverse jet flowfield found that, in addition to the thrust force of the fluid injected into the primary stream, the complex pressure field resulting from the jet-crossflow interaction provided an additional aerodynamic force normal to the surface through which the jet was injected. Although extensive pressure data were obtained in early studies of this problem, such as that by Cubbison et al.[1] and Janos,[2] the effects of jet injection over the entire control surface were of primary interest. As a result of this interest in the far-field effects, pressure taps were generally located at least 3–5 jet diameters away from the injector port. More recently, several analytical and numerical investigations of this jet-interaction flowfield have been undertaken.[3–5] Reasonable agreement with gross flowfield features, such as the penetration height of the jet, has usually been obtained.

An additional application of current interest for a transverse jet is as a fuel injector for a supersonic combustor. The development of supersonic combustors has been motivated by the desire to develop an air-breathing hypersonic aircraft. For such an aircraft to operate efficiently, the flow velocity through the combustor must be supersonic, and losses resulting from the presence of shock waves must be minimal. In addition, for the injected fluid to mix well with the primary stream, the jet must have sufficient momentum to penetrate into the freestream. Because the trajectory of the injectant downstream of the Mach disk is nearly parallel to the surface through which the jet is injected, the height of the Mach disk above this surface has served as a measure of jet penetration into the freestream.

As a result of an investigation performed by Zukoski and Spaid,[6] an analytical model was developed by applying an integral momentum balance to predict the penetration of the injectant into the freestream. Simplifying assumptions made for this model included neglect of the crossflow boundary layer, no mixing of the injectant and freestream in the near field, and an assumed shape for the injected fluid trajectory. The governing parameters for prediction of the penetration height of the injectant were the freestream Mach number and static pressure, as well as the injectant mass flow rate, stagnation temperature, and gas constant.

Schetz and Billig[7] introduced the concept of an effective back pressure surrounding the injected jet. This back pressure is analogous to that around a jet injected into quiescent air. The complexity of the flowfield around the injector port and the difficulty in adequately measuring the pressure near the jet

Received Dec. 19, 1997; revision received May 10, 1998; accepted for publication May 25, 1998.

*Project Engineer, St. Joseph Technical Center.
†Graduate Research Assistant, Department of Mechanical and Industrial Engineering. Student Member AIAA.
‡W. Grafton and Lillian B. Wilkins Professor, Department of Mechanical and Industrial Engineering. Associate Fellow AIAA.
§Associate Professor, Department of Mechanical Engineering. Member AIAA.

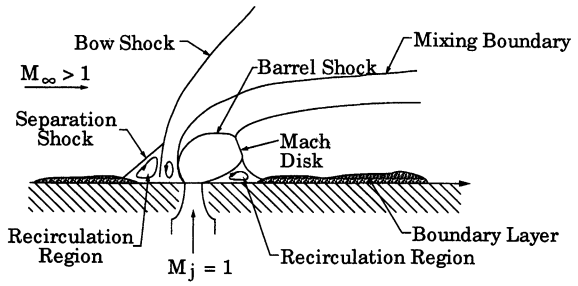

Fig. 1 Flowfield schematic.

orifice make experimental determination of this back pressure difficult. Therefore, assumptions for the back pressure were made depending upon whether the boundary-layer thickness along the wall at the injector location was greater than or less than the orifice diameter. For cases in which the boundary-layer thickness was less than the injector diameter, the effective back pressure was assumed to be one-half the stagnation pressure behind a normal shock in the freestream. When the boundary-layer thickness was greater than the orifice diameter, on the other hand, the effective back pressure was assumed to be one-half the static pressure in the separated region immediately upstream of the jet. As a result of this study, penetration of the jet was found to be controlled primarily by the magnitude of the jet-to-crossflow momentum flux ratio, J, defined as

$$J \equiv \frac{(\rho V^2)_j}{(\rho V^2)_\infty} = \frac{(\gamma p M^2)_j}{(\gamma p M^2)_\infty} \tag{1}$$

For large values of J, it was suggested that penetration could be enhanced by matching the jet exit pressure to that of the effective back pressure; underexpanded conditions decreased the penetration of the jet at high values of J because of the loss of jet momentum as the flow passes through the Mach disk.

Further study of the effects of momentum flux ratio, jet injectant pressure, and jet Mach number were performed by Orth and Funk.[8] For these experiments, the effective back pressure was taken to be the average static pressure around a cylindrical object on a flat plate in a supersonic flow, namely, two thirds of the stagnation pressure of the freestream behind the bow shock. Conclusions from this study were that increasing the injectant exit pressure above that of the effective back pressure did little to increase the penetration of the jet into the freestream for a fixed value of J. In further work by Schetz et al.,[9] the adequacy of the effective back-pressure concept was tested by correlating the height of the Mach disk (normalized by the jet diameter) with the ratio of jet pressure-to-effective back pressure for injection into both a supersonic stream and quiescent air. These data were seen to correlate well for an effective back pressure equal to 0.8 of the static pressure behind a normal shock in the freestream.

Billig et al.,[10] using an estimate of the effective back pressure equal to two thirds of the stagnation pressure behind a normal shock in the freestream, developed a correlation to predict the height of the Mach disk, y, as a function of the effective back pressure, jet pressure, diameter of the injector throat, and jet Mach number. This relationship is of the form

$$\frac{y}{d^*} = M_j^{1/4} \left(\frac{p_j^*}{p_{eb}}\right)^{1/2} \tag{2}$$

where the asterisks denote conditions at the jet throat. This study also found that when the mass flow rate of the jet was held constant, increasing the injection pressure of the jet had little effect on the absolute penetration of the jet.

More recently, Papamoschou et al.[11] focused an investigation on pressure-matched jets, for which the jet exit pressure was determined, or matched, by varying it until the minimum amount of shock structure in the jet was observed visually. Under these conditions, the jet exit pressure was considered to be matched with the effective back pressure. In this manner, an effective back pressure of 0.3 of the static pressure behind a normal shock in the freestream was found to optimize penetration height of the injectant.

The complexity of the flowfield around the injector port resulting from the jet–crossflow interaction and the difficulty of placing a large number of pressure taps around the periphery of the orifice have made accurate determination of the surface pressure distribution in the immediate neighborhood of the injector difficult. Because of this difficulty, a number of estimates of effective back pressure, as previously described, have been used in developing predictions of jet penetration and other parameters of interest. In this investigation, pressure-sensitive paint (PSP) was used to determine the continuous surface pressure field about a sonic jet injected transversely into a Mach 1.6 freestream for several flow conditions. From this knowledge of the pressure field, the pressure distribution around the jet periphery and the effective back pressure were determined.

Experimental Facilities

The experiments described herein were performed in the blowdown wind-tunnel facilities of the Gas Dynamics Laboratory at the University of Illinois at Urbana–Champaign. A planar two-dimensional wind tunnel, with a freestream Mach number of 1.6 and dimensions at the location of jet injection of 76 mm wide by 36 mm high, was used in this study. The test section was constructed of aluminum and sealed with O-rings and vacuum grease. Optical access in the wall opposite the injector port was provided by a fused silica window epoxied into the wall.

The sonic jet was injected normal to the freestream through a 4-mm-diam circular hole in the upper wall of the test section. A convergent nozzle with sonic exit velocity for the transverse jet was used in this investigation. The jet nozzle contour was that of a 3:5 (minor-to-major axis) ellipse; the minor axis was oriented parallel to the flow. The injection site for the jet was chosen at a location where the boundary-layer thickness of the freestream approximately equaled that of the jet diameter. The boundary-layer thickness along the length of the Mach 1.6 test section was determined previously by Carroll.[12] Conventional pressure taps were placed around the jet orifice: 7 along the jet centerline upstream of the orifice, 7 downstream of the orifice, and 10 off-centerline taps in the near-jet flowfield. The pressures at these locations were determined using a Pressure Systems DPT-6400 multichannel digital pressure transmitter.

Air for the freestream flow was supplied by a high-pressure, compressed-air tank farm that was fed by two compressors, an Ingersoll–Rand and a Gardner–Denver, capable of delivering 61 kg/min of air at an average pressure of 841 kPa. The stagnation pressure and stagnation temperature for the crossflow were 241 kPa and 300.1 K, respectively, in all experiments. Air to the transverse jet was supplied by six size-T compressed gas bottles connected together by a six-station bottle manifold. For the experiments reported in this paper, the injectant stagnation pressures were 330, 468, and 606 kPa, and the stagnation temperature was 300.1 K. The resulting jet-to-crossflow momentum flux ratios were $J = 1.2$, 1.7, and 2.2, respectively.

Diagnostic Methods

Qualitative information about the transverse jet flow was obtained using shadowgraph photography as well as surface oil-flow visualization. Shadowgraph visualization was used to examine the qualitative features of the flowfield. A spark light source with an approximate pulse duration of 20 ns was used to illuminate the flowfield. A Nikon F2 35-mm SLR camera

using Kodak T-MAX 3200 black-and-white film was used to record the shadowgraph images.

Surface oil-flow visualization was also performed to determine separation and reattachment information in the near-jet region. A mixture of STP® Oil Treatment, kerosene, and lampblack was used as the surface tracer in these studies. Experiments with the mixture applied to the entire surface around the injector port, as well as experiments with the mixture applied as a matrix of discrete dots, were performed. A final series of surface flow experiments involved applying the mixture in a line upstream of the jet and observing the flow patterns and separation regions as the mixture approached the jet port. The flow patterns established in each of these experiments were recorded by applying a 2-in. strip of clear adhesive tape over the surface streaklines and pulling them from the tunnel wall.

The primary diagnostic tool used in this study was PSP. PSP is a relatively new optically based diagnostic technique for determining absolute static pressure distributions on a surface.[13–15] PSP utilizes the fluorescence of organic luminophores (probe molecules) suspended in polymeric binders. The luminophores are excited using an excitation light source with a visible bandpass filter. The diffusion of oxygen through the polymeric binder locally quenches the fluorescence of these luminophores suspended in the binder. With the local concentration of oxygen related to the local static pressure through Henry's law, it is evident that pressure is inversely proportional to the luminescent intensity of the PSP. The intensity of the PSP's fluorescence is captured with a scientific-grade charge-coupled device (CCD) camera. An emission bandpass filter, placed on the front of the CCD camera lens, separates the fluorescence of the paint from the light of the excitation source. Pressure measurements are obtained through pixel-by-pixel division of an image of the PSP-treated surface at flow-off (reference) conditions, usually chosen to be atmospheric pressure and temperature, with an image at flow-on (run) conditions. Knowledge of the PSP intensity ratio, I_{ref}/I_{run}, obtained experimentally at several known pressures (measured by conventional pressure taps and transducers), allows an in situ PSP calibration curve to be created. Thus, through this calibration curve, the static pressure at any point on the surface can be calculated using the normalized intensity (I_{ref}/I_{run}) of the PSP at that point.

The basic PSP measurement equipment employed in these experiments and the wind-tunnel test section are illustrated in Fig. 2. While numerous PSP formulations exist in the literature, the paint chosen for these experiments was based upon the PSP study conducted by Woodmansee and Dutton,[16] who found that a ruthenium-based PSP from Old Dominion University (ODU PSP) provided adequate pressure sensitivity and limited temperature sensitivity for conditions often found in supersonic wind tunnels. Furthermore, compared to other industrially developed PSPs, the ODU PSP formulation is publicly available.[16]

Obviously, the bandpass filters chosen for the PSP measurements depend upon the excitation and emission wavelengths of the probe molecule in the PSP. For the ODU PSP illumination spectrum, a Melles Griot 03 FIV 028 Visible 40 dichroic bandpass filter centered at 450 nm was used. A Melles Griot 03 FIB 012 Visible 80 dichroic bandpass filter centered at 600 nm was selected as the ODU PSP detection filter. A light source, specifically manufactured for luminescent measurements, was used to excite the PSP. The aluminum light source housed a 75-W tungsten–halogen light bulb. A lip at the front of the housing held the glass excitation bandpass filter, allowing only filtered light to illuminate the painted surface. To maintain the light source at a constant temperature, forced-air cooling was provided through 1/8-in. threaded holes in the housing; these holes were located between the filter and light bulb, allowing the piped air to adequately cool the inner components and the housing itself.

To make quantitative measurements using PSP, an imaging device must be used that is capable of providing high spatial resolution of the surface under investigation, as well as responding uniformly to changing light intensities. A scientific grade, unintensified CCD camera was chosen for this study. The camera system used was a Photometrics, Ltd. Series 200 14-bit system with thermoelectric cooling to reduce electrical and thermal noise. The detector utilized was a back-illuminated, thinned Tektronix TK512CB/AR-M array with 512 × 512 pixel resolution. The use of a 14-bit camera provided high resolution for light intensity variations. The bandpass emission filter was placed on the front of the camera lens using a modified 35-mm camera gel filter mount. The camera system was controlled by the Photometrics Imaging Software (PMIS) package run on an IBM-compatible 80486 computer. Subsequent image processing was performed using a suite of Fortran routines devised specifically for luminescent coating experiments.[17]

Results

Shadowgraph

A series of shadowgraph photos was obtained to verify that the flowfield structure was as expected and to determine qualitative information about the transverse jet flow. Figure 3 illustrates a result of these experiments for $J = 1.7$. The general characteristics of the flowfield are evident in this photograph. Upstream of the jet injection site is the separation shock and the bow shock. As the jet is injected into the crossflow, it first expands through a Prandtl–Meyer fan centered at the nozzle lip; the jet flow is then compressed as it passes through either the sides of the barrel shock or the Mach disk.

Comparison of these flow features from the shadowgraphs for each case indicated several trends. As the jet-to-crossflow momentum flux ratio, J, was increased, the distance between

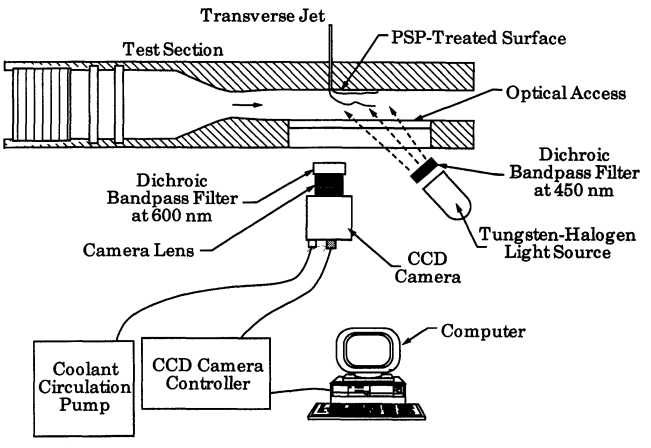

Fig. 2 Test section and PSP imaging schematic.

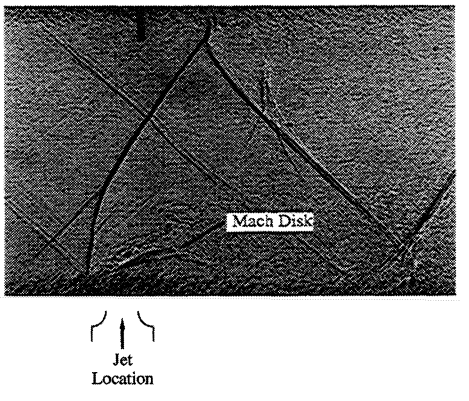

Fig. 3 Shadowgraph for $J = 1.7$.

the projected intersection of the separation shock with the wall and the projected intersection of the bow shock with the wall increased. The height of the intersection of the separation shock and the bow shock from the injector port wall also increased with increasing J. The strength of the bow shock, as indicated by its inclination to the crossflow, was also seen to increase with increasing J and approached the strength of a normal shock for a larger distance normal to the wall. As the ratio of the injectant static pressure to the freestream static pressure increased [increasing J for fixed freestream and jet Mach numbers; see Eq. (1)], the size of the barrel shock region increased and the height and size of the Mach disk also were seen to increase.

Surface Oil-Flow Visualization

After having verified the flowfield characteristics through the shadowgraph photos, surface oil-flow visualization was performed at each of the experimental conditions for qualitative comparison to the surface pressure measurements. The results of these experiments are illustrated in Fig. 4 for the J = 1.2 case. By applying the surface tracer mixture upstream of the injector port, two separation lines, or Γ lines, were identified that wrapped around the injector (Fig. 4). The distinctive shape of these Γ lines has led previous investigators to refer to the vortex system resulting from the flow separation in this region as the horseshoe vortex. Immediately downstream of each of the Γ separation lines, along the tunnel centerline and upstream of the injector, a region of recirculating flow was observed. The oil between the two Γ lines was not observed to penetrate either Γ line as it moved outward and around the jet. Inside the second, inner Γ line, the oil also did not penetrate the second Γ line as it moved around the jet.

At the downstream boundary of the jet orifice, another region of separation occurred where oil was observed to pool. From this point of separation, two lines were formed along which oil accumulated. These are referred to as Δ lines and were observed to be a boundary between the flow upstream of the jet that moved around the jet and the reattaching flow downstream of the injector port. Initially, the Δ lines were observed to diverge as they progressed downstream. For the J = 1.2 case, the Δ lines continued to diverge until approximately three jet diameters downstream of the orifice, after which they were observed to converge slightly before continuing straight downstream. For the higher J cases, the Δ lines diverged until intercepting the inner Γ line as it wrapped around the jet injector port.

Between the two Δ lines, a node of attachment was observed. From this point, the flow moved radially outward toward the Δ lines, where the flow was directed along the corresponding Δ line and then eventually downstream.

Pressure Sensitive Paint

Having obtained qualitative flow visualization information about the transverse jet flowfield through the shadowgraph and oil-flow experiments, PSP was applied to the near-jet surface to obtain quantitative information concerning the surface pressure distribution about the jet. As described earlier, experimental data were obtained for the three jet-to-crossflow momentum flux ratios: J = 1.2, 1.7, and 2.2. For each case, 20 run images and 20 reference images were acquired; the reference images were taken immediately after the flow had been shut off to minimize temporal temperature variations along the tunnel wall between flow-on and flow-off conditions. The 20-image sequences were then ensemble-averaged and the dark noise subtracted, providing a single run image and a single reference image for each J condition.

Based on observation of the known jet diameter in the images, the spatial resolution of the measurements on the surface was calculated to be 85.1 μm/pixel edge or approximately 89,000 pressure measurements per square inch. With this resolution, the PSP-painted area imaged by the CCD camera extended from approximately 3.5 jet diameters upstream of the orifice center to 4.5 jet diameters downstream with a spanwise half-width of approximately four jet diameters.

During the experiment, the PSP images and pressure tap measurements were acquired simultaneously. As discussed next, the pressure tap measurements were used in conjunction with the PSP images to form an ODU PSP calibration curve for each J condition. For the ensemble-averaged images, the 1.02-mm-diam pressure taps appeared as dark circles, approximately 12 pixels in diameter. These pressure taps provided excellent reference marks with which to align the run image to the reference image. To account for the wind-tunnel shift during flow-on conditions, a subpixel image alignment algorithm[17] was used to calculate the geometrical centroids of the pressure taps in the reference and run images. The code compared the relative location of each tap in both images and then shifted the entire run image back to the reference image using a subpixel linear–interpolation routine. The shift, based upon the average difference between the pressure tap centroids in the reference and run images, was approximately 0.1 and 1.3 pixels in the streamwise and spanwise directions, respectively.

From the aligned average reference (I_{ref}) and run (I_{run}) images, an image representing the intensity ratio (I_{ref}/I_{run}) for each experimental case was calculated. To eliminate the images of the pressure taps from these intensity ratio results, a pressure tap masking scheme[17] was employed. Using the intensity ratios of the pixels surrounding the pressure tap as boundary conditions, a two-dimensional paraboloid with six undetermined coefficients was fit in a least-squares manner over each pressure tap surface. Instead of relying on pixels around the perimeter of the tap to estimate the average I_{ref}/I_{run} values used in the PSP calibration curve, the average I_{ref}/I_{run} value of the paraboloid fit was utilized. This intensity ratio was then related to the pressure measured at the tap by the pressure transmitter. Hence, an in situ[13,15–17] calibration curve was created by relating the pressure and PSP intensity ratio (I_{ref}/I_{run}) measured at each tap throughout the flowfield.

Figure 5 is the in-situ calibration curve used for the J = 1.2 condition. As suggested by the correlation coefficient, R = 0.995, a second-order polynomial[18] fits the data quite well. Two of the possible 24 pressure tap calibration points are miss-

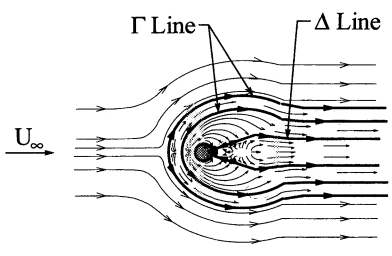

Fig. 4 Oil-flow schematic for J = 1.2.

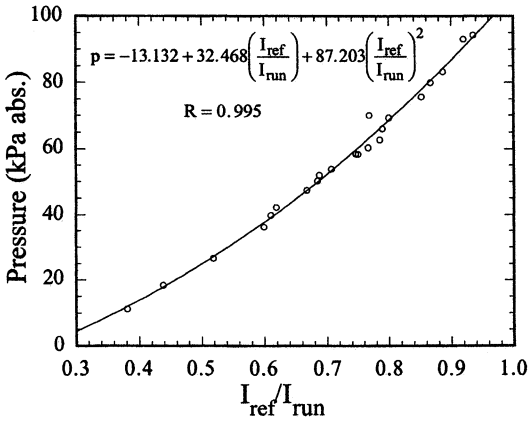

Fig. 5 In situ calibration curve for J = 1.2; uncertainty in p = ±1 kPa.

ing from Fig. 5 because 1) one tap fell outside the CCD camera image area and 2) another tap had a faulty vinyl tube connecting it to the multichannel pressure transmitter. It is evident from this plot that the taps encompass a wide range of pressures in the near-jet flowfield. Figure 5 emphasizes the importance of placing taps in the regions of extreme pressures, thereby minimizing any extrapolation of pressures from I_{ref}/I_{run} values that fall outside the range determined by the in situ calibration curve. Moreover, it is also imperative that a number of taps be placed in locations between the maximum and minimum pressures, so as to accurately define the shape of the calibration curve.

Figure 6 presents the normalized streamwise wall pressure distribution along the tunnel spanwise centerline for the J = 1.2 case. The freestream static pressure, p_∞, used to normalize the pressures was calculated using the isentropic flow relation for a freestream Mach number of 1.6 and the freestream stagnation pressure measured during the experimental runs. This value agreed closely with pressure tap measurements made far upstream of the orifice. The horizontal error bars on the pressure tap measurements represent the diameter of the taps in relation to the jet orifice diameter. Vertical error bars are unnecessary, as the uncertainty of the pressure tap measurements was 1 kPa, approximately the same as the diameter of the markers themselves. Starting at about three jet diameters upstream of the injector port centerline, the pressure is observed to increase steadily until approximately one jet diameter upstream of the injector centerline, where a sudden increase in pressure is observed. Comparison of these locations with the shadowgraph photo for J = 1.2 indicates that the increase in pressure starting three diameters upstream and the sudden increase in pressure one diameter upstream correspond to the locations of the separation shock and the bow shock, respectively. Immediately downstream of the injector on the centerline, a region of extremely low pressure is present where the injected fluid has caused the freestream flow about the jet to separate. As the flow along the centerline continues downstream, it is recompressed until it approaches the freestream static pressure. In Fig. 6, the unusual decrease in the p/p_∞ profile at about x/d_j = 4 is the result of a flaw in the wall caused by previous planar laser-induced fluorescence experiments; it is evident that even small surface imperfections in the PSP-coated surface can have a pronounced effect on the final PSP pressure distribution.

In Fig. 6, the PSP measurements generally follow the centerline pressure tap measurements quite closely both upstream and downstream of the jet. This is particularly true in the downstream region where the PSP pressure distribution and the discrete pressure tap measurements are virtually identical through the separation and recompression regions. Along the centerline, the largest absolute difference between the PSP and transducer measurements occurs just upstream of the jet orifice between the bow shock and the front lip of the orifice. At this location, the PSP-measured pressure is 7 kPa below the tap pressure of 94 kPa. This corresponds to a 7.9% difference (based on the transducer measurement). Comparison of the PSP and conventionally measured pressures along the centerline indicate an rms pressure difference of 3 kPa. The largest percentage difference (10.4%) occurs at the pressure tap just downstream of the jet; however, this large percentage difference is a result of the low pressures (11 kPa) in this separated area. Hence, to identify the pressure discrepancies between the PSP and pressure tap measurements, absolute differences (in kPa) rather than percentage differences are used. Possible sources of the differences between the PSP measurements and the tap measurements could stem from small misalignments in the ratioed images, temperature variations across the flowfield, errors in the pressure tap masking algorithm, and variations in the pixel-to-pixel gain of the CCD camera.

Figure 7 presents a comparison of the normalized centerline pressure distributions for the three experimental cases. This plot indicates several trends. For each of the higher momentum flux ratio cases, as in the low J case, a region of steadily increasing pressure upstream of the injector is present, corresponding to the location of the recirculation region between the separation shock and the bow shock. In addition, a region of sharply increasing pressure immediately behind the bow shock occurs for all three cases. As J increases, the region of increasing pressure between the separation shock and the bow shock extends farther upstream, as does the region of very high pressure behind the bow shock. This agrees qualitatively with information obtained from the shadowgraph images. The peak static pressure immediately behind the bow shock can also be seen to increase with increasing J. As observed in the shadowgraph visualizations, the strength of the bow shock, as judged by its obliquity to the crossflow, increases with increasing jet-to-crossflow momentum flux ratio, J. Because of this increase in the strength of the bow shock, it is therefore reasonable to expect that the static pressure behind the bow shock would also increase and be limited by the static pressure behind a normal shock at the freestream Mach number (p_2/p_∞ = 2.82).

Downstream of the injector port, a region of low pressure is also present for the higher J cases, as in the J = 1.2 case. For the J = 1.2 and 1.7 cases, as the flow progresses through the separated region and into the recompression region, the pressure steadily increases until it approaches the freestream static pressure (p/p_∞ = 1.0). In the J = 2.2 case, however, the surface pressure increases past the freestream static pressure because of the presence of the reflection of the bow shock from the top wall of the tunnel. This reflected shock is evident in the shadowgraph photograph of Fig. 3. As the stagnation pressure, i.e., J, of the transverse jet is increased, the impingement point of the reflected shock on the bottom wall moves

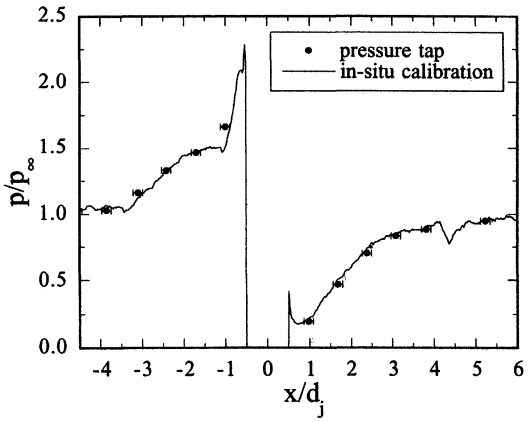

Fig. 6 Centerline pressure distribution for J = 1.2; uncertainty in p/p_∞ for pressure tap data is ±0.02 and for PSP data is ±0.05.

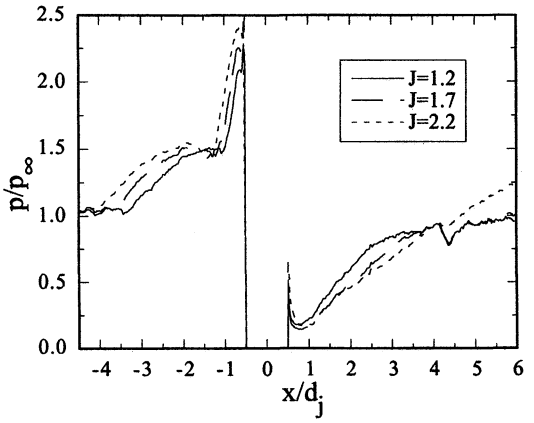

Fig. 7 Comparison of centerline pressure distributions; uncertainty in p/p_∞ = ±0.05 for all cases.

upstream toward the transverse jet. In the $J = 2.2$ case, the impingement point of the reflected shock was far enough upstream to affect the recompression process along the jet centerline, as seen in Fig. 7. For each of the three experimental cases examined, the distance downstream at which the pressure reaches the freestream pressure increases with increasing J. For the $J = 1.7$ and 2.2 cases, excellent agreement between the PSP-calculated pressures and the transducer-measured pressures (not shown) in the separation and recompression regions downstream of the injector was obtained. However, the PSP-measured pressures upstream of the injector for the higher J cases were observed to deviate slightly from the transducer-measured pressures, as in the $J = 1.2$ case shown in Fig. 6. Moreover, the largest absolute difference in pressure (11 kPa for $J = 1.7$, 9 kPa for $J = 2.2$) between the PSP and pressure tap measurements occurred at the first tap upstream of the injector port ($x/d_j = -1$).

Figure 8 is a color contour plot of the surface static pressure distribution in the near-jet region for the $J = 1.2$ case. Because of the symmetrical nature of this flowfield, only half of the surface pressure distribution is presented here. The flow direction in this image is from top to bottom with the transverse jet evident as a dark semicircle at the origin of the image. Again, the pressures are normalized by the freestream static pressure. Moving downward along the jet centerline in Fig. 8, the two high-pressure regions caused by the separation shock and the bow shock are evident as curved bands that wrap around the front of the orifice. The first high-pressure region ($-2 \leq x/d_j \leq -1$ at the centerline), which is caused by the separation shock, is the larger of the two and extends nearly 90 deg off the transverse jet center. The foot of the curved bow shock ($x/d_j \approx -1$ along the centerline) resides between the first and second high-pressure regions. This shock causes a dramatic increase in pressure in the second crescent-shaped recirculation region that extends to the front lip of the jet orifice. The pressure within this second recirculation region reaches above-ambient conditions as the freestream is forced to decelerate to a near-zero velocity in the stagnation region in front of the jet.

Behind the jet orifice, a low-pressure region extends approximately 2.5 jet diameters downstream along the tunnel centerline. By four jet diameters past the orifice center, recompression to the freestream surface pressure is obtained. Interestingly, a low-pressure wing, approximately 30 deg off the centerline axis, extends the recompression region farther downstream than along the centerline. Clearly, the advantages of using PSP for surface pressure measurements are evident in Fig. 8, as it demonstrates PSP's superior spatial resolution in this highly varying pressure field.

Figure 9 illustrates the pressure map for the $J = 1.7$ experimental conditions. Comparison of this image to Fig. 8 indicates that, in addition to the region of increased pressure behind the separation shock extending further upstream than in the $J = 1.2$ case, this region of higher pressure extends farther in the spanwise direction as well. The former effect was also observed in the comparison of the centerline pressure distributions. The high static pressure immediately behind the bow shock is also greater in magnitude and spatial extent than that of the low J case. Downstream of the injector port, the region of low pressure can also be seen to extend farther downstream than in the low J experiments. Although the pressure gradient in the region of the bow shock is much greater, and the low-pressure region is larger in spatial extent for this experimental condition than that illustrated in Fig. 8 for $J = 1.2$, the expansion about the jet injector port appears to be quite similar for these two cases.

The results of the PSP measurements for the $J = 2.2$ case are presented in Fig. 10. Again, as J is increased above the intermediate value, the peak static pressure behind the bow shock also increases, as does the size of the region upstream of the jet injector of increased pressure between the bow and separation shocks. Downstream of the injector port, the region of low pressure also extends further downstream at this highest J condition.

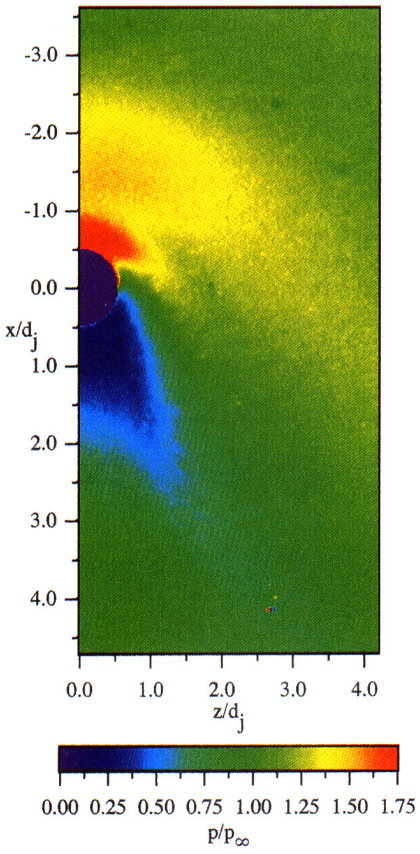

Fig. 8 $J = 1.2$ pressure distribution; uncertainty in $p/p_\infty = \pm 0.05$.

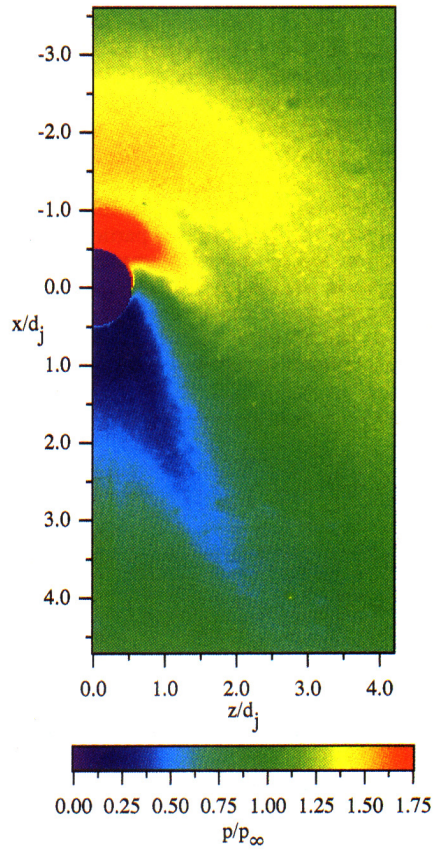

Fig. 9 $J = 1.7$ pressure distribution; uncertainty in $p/p_\infty = \pm 0.05$.

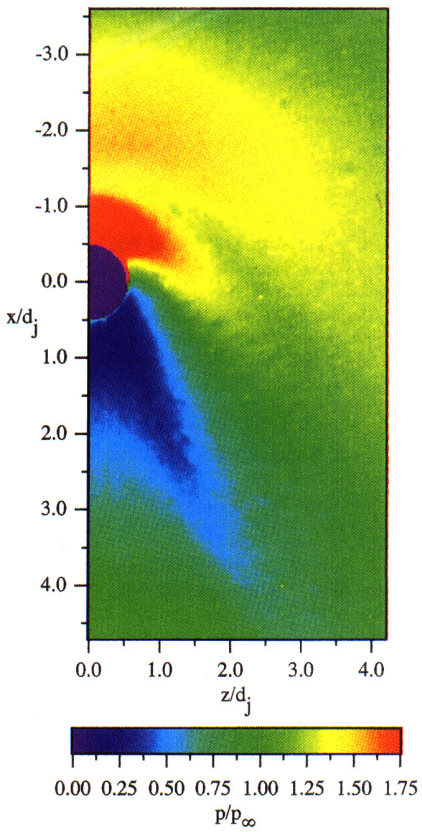

Fig. 10 J = 2.2 pressure distribution; uncertainty in p/p_∞ = ±0.05.

Effective Back Pressure

After the surface pressure distributions for the three experimental cases were obtained, the determination of the effective back pressure, p_{eb}, about the injector port was examined. In this study the effective back pressure, p_{eb}, is defined as the circumferentially averaged surface pressure about the orifice

$$\frac{p_{eb}}{p_2} = \frac{1}{\pi}\int_0^\pi \frac{p(\theta)}{p_2}\,d\theta \tag{3}$$

where p_2 is the static pressure behind a normal shock in the freestream, and θ is the circumferential angle in radians. While this definition of p_{eb} obviously cannot account for off-surface effects about the jet plume, it does control the initial strength of the expansion waves centered at the orifice lip and, therefore, the initial jet structure.

Care was taken to choose an annular ring of pixels around the jet orifice that captured the extreme pressures before and after the jet, but which omitted any surface imperfections that commonly occur near sharp corners or holes like the transverse jet orifice. A parametric study of this effect was conducted by extracting annular rings of pixels concentric with the jet orifice (each ring being one pixel wide) and comparing the rings' pressure profile over the range $0 \le \theta \le \pi$. From this study, it was concluded that an annular ring 0.34 mm (four pixel widths) from the jet lip should be used, providing 90 discrete PSP pressure measurements. This ring of pixels captured the extreme pressures around the jet orifice without including unwanted edge effects or major surface imperfections.

The PSP pressure measurements at the jet periphery normalized by the static pressure behind a normal shock at the freestream Mach number (p_2) are presented in Fig. 11 for all three jet-to-crossflow momentum flux ratios. The pressure distribution is seen to decrease smoothly around the periphery of the jet for all three cases before reaching a low and relatively

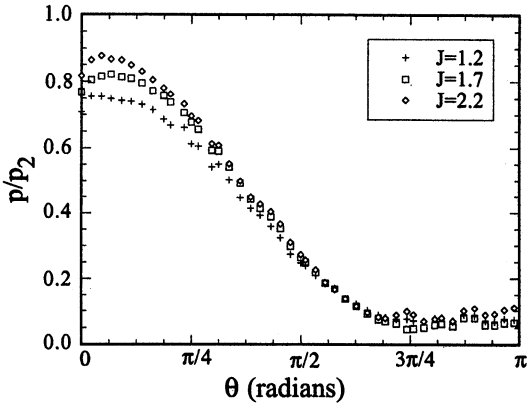

Fig. 11 Comparison of circumferential pressure distributions; uncertainty in p/p_2 = ±0.02 for all cases.

constant value on the downstream side of the orifice for $3\pi/4 \le \theta \le \pi$. The expansion of the flow about the jet periphery is nearly identical for the three cases, except near the leading edge of the orifice where the static pressure behind the bow shock is observed to increase with increasing J. The small drop in pressure at the $\theta = 0$ upstream edge of the jet for all three cases is caused by a small flaw in the paint in this region. The pressure at the $\theta = 0$ location should actually be near the peak values measured just off the centerline.

The pressure taps used to obtain the in situ calibration were placed in or near locations of extremes of the surface pressure distribution. Unfortunately, as shown by Fig. 6, the highest surface pressure occurs immediately before the front lip of the transverse jet, where machining a tap is extremely difficult. Hence, when converting I_{ref}/I_{run} values to pressure, approximately 26% (23 out of 90 pixels) of the I_{ref}/I_{run} values in the annular ring around the transverse jet fell outside the pressure tap measurement range; these values were determined by extrapolation of the in situ calibration curve. While this may be a cause for concern, Woodmansee and Dutton[16] considered other techniques that used only interpolation of separately obtained calibration data and/or explicit compensation for temperature effects, only to find the in situ data reduction method to be the most accurate calibration technique. Also, the fact that the second-order polynomial fits the 22 calibration points with a high correlation coefficient, as shown in Fig. 5, leads one to believe that the pressures determined from the extrapolation will be predicted by the polynomial almost as accurately as interpolated values.

The calculated values of the effective back-pressure ratio, determined by integrating [Eq. (3)] the pressure distributions shown in Fig. 11, for the three experimental cases examined herein were, in order of increasing J, p_{eb}/p_2 = 0.343, 0.361, and 0.383. As observed in Fig. 12, the effective back pressure for these three conditions increases approximately linearly with increasing momentum flux ratio over the range investigated. This increase is clearly a result of the higher pressures near the upstream edge of the injector for the higher J, as shown in Figs. 7 and 11.

Comparison of the effective back pressure determined in these experiments with the wide range of empirical values used in previous theories and experiments results in various degrees of agreement. The best agreement between the effective back pressure determined here and previous estimates is the $p_{eb} = 0.3p_2$ value given by Papamoschou et al.[11] The estimates of $0.8p_2$ and $0.67p_{02}$ ($p_{02} = 1.35p_2$ for $M_1 = 1.6$) used by other investigators (Schetz and Billig,[7] Orth and Funk,[8] and Schetz et al.[9]) differ greatly from the effective back pressures determined in the current experiments. However, as discussed in the Introduction, the definitions of effective back pressure used by various investigators differ, which accounts for these discrepancies. In addition, the previous experiments reported in

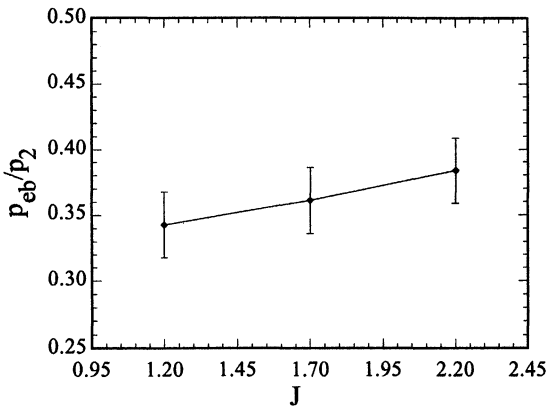

Fig. 12 Effective back-pressure variation with J; uncertainty in $p_{eb}/p_2 = \pm 0.025$.

Refs. 7–9 were generally performed at much larger values of the momentum flux ratio than for the current study, whereas the experiments of Papamoschou et al.[11] were nearer the experimental conditions used here. On the other hand, the current experiments show that p_{eb}/p_2 increases with J, albeit rather weakly, which is an effect not included in any of the previous empirical estimates of effective back pressure.

Conclusions

Application of the PSP technique to the flowfield resulting from a sonic jet injected transversely into a supersonic stream revealed several characteristics of the surface pressure distribution. In the region between the bow shock and the leading edge of the injector port, the surface static pressure was observed to be dependent upon the jet-to-crossflow momentum flux ratio, i.e., the peak static pressure increased with increasing J. Upstream of the bow shock, the size of the region between the bow and separation shocks was also observed to increase with increasing J.

As the flow passed around the injector port, the flow expanded from the high-pressure region between the bow shock and the injector port to a low-pressure separation region at the downstream edge of the injector. Aside from the initial high-pressure differences in the upstream region of the injector orifice, the expansion around the periphery of the injection site was observed to be essentially independent of momentum flux ratio. Downstream of the injector, a region of low pressure was observed, which increased in overall size as well as streamwise extent with increasing J.

The circumferential pressure distribution at the edge of the injector port was integrated to determine a value for the effective back pressure about the jet periphery. This effective back pressure was observed to increase modestly with increasing J as a result of the increase in the static pressure at the leading edge of the jet. Comparison of the estimates of the effective back pressure used by previous investigators to those determined in this study indicates that estimation of the effective back pressure as a constant fraction of the static or stagnation pressure behind a normal shock in the freestream is erroneous, at least over the range of J studied here, because of the aforementioned dependence on J.

Acknowledgments

This work was supported by Grant DAAL03-93-G-0143 from the U.S. Army Research Office with Thomas L. Doligalski as the Monitor.

References

[1]Cubbison, R. W., Anderson, B. H., and Ward, J. J., "Surface Pressure Distributions with a Sonic Jet Normal to Adjacent Flat Surfaces at Mach 2.92 to 6.4," NASA TN D-580, 1961.

[2]Janos, J. J., "Loads Induced on a Flat-Plate Wing by an Air Jet Exhausting Perpendicularly Through the Wing and Normal to a Free-Stream Flow of Mach Number 2.0," NASA TN D-649, 1961.

[3]Heister, S. D., and Karagozian, A. R., "Vortex Modeling of Gaseous Jets in a Compressible Crossflow," *Journal of Propulsion and Power*, Vol. 6, No. 1, 1990, pp. 85–92.

[4]Heister, S. D., and Karagozian, A. R., "Gaseous Jet in Supersonic Crossflow," *AIAA Journal*, Vol. 28, No. 5, 1990, pp. 819–827.

[5]Uenishi, K., and Rogers, R. C., "Three-Dimensional Computation of Mixing of Transverse Injector in a Ducted Supersonic Airstream," AIAA Paper 86-1423, June 1986.

[6]Zukoski, E. E., and Spaid, F. W., "Secondary Injection of Gases into a Supersonic Flow," *AIAA Journal*, Vol. 2, No. 10, 1964, pp. 1689–1696.

[7]Schetz, J. A., and Billig, F. S., "Penetration of Gaseous Jets Injected into a Supersonic Stream," *AIAA Journal*, Vol. 3, No. 11, 1966, pp. 1658–1665.

[8]Orth, R. C., and Funk, J. A., "An Experimental and Comparative Study of Jet Penetration in Supersonic Flow," *Journal of Spacecraft and Rockets*, Vol. 4, No. 9, 1967, pp. 1236–1242.

[9]Schetz, J. A., Hawkins, P. F., and Lehman, H., "Structure of Highly Underexpanded Transverse Jets in a Supersonic Stream," *AIAA Journal*, Vol. 5, No. 5, 1967, pp. 882–884.

[10]Billig, F. S., Orth, R. C., and Lasky, M., "A Unified Analysis of Gaseous Jet Penetration," *AIAA Journal*, Vol. 9, No. 6, 1971, pp. 1048–1058.

[11]Papamoschou, D., Hubbard, D. G., and Lin, M., "Observations of Supersonic Transverse Jets," AIAA Paper 91-1723, June 1991.

[12]Carroll, B. F., "A Numerical and Experimental Investigation of Multiple Shock Wave/Turbulent Boundary Layer Interactions in a Rectangular Duct," Ph.D. Dissertation, Dept. of Mechanical and Industrial Engineering, Univ. of Illinois at Urbana–Champaign, Urbana, IL, 1988.

[13]Kavandi, J. L., "Luminescence Imaging for Aerodynamic Pressure Measurements," Ph.D. Dissertation, Department of Chemistry, Univ. of Washington, Seattle, WA, 1990.

[14]Morris, M. J., Donovan, J. F., Kegelman, J. T., Schwab, S. D., Levy, R. L., and Crites, R. C., "Aerodynamic Applications of Pressure-Sensitive Paint," AIAA Paper 92-0264, Jan. 1992.

[15]Morris, M. J., Benne, M. E., Crites, R. C., and Donovan, J. F., "Aerodynamic Measurements Based on Photoluminescence," AIAA Paper 93-0175, Jan. 1993.

[16]Woodmansee, M. A., and Dutton, J. C., "Treating Temperature-Sensitivity Effects of Pressure-Sensitive Paint Measurements," *Experiments in Fluids*, Vol. 24, No. 2, 1998, pp. 163–174.

[17]Woodmansee, M. A., "Temperature-Sensitivity Effects of Pressure-Sensitive Paint and Associated Wind Tunnel Data Reduction Methods," M.S. Thesis, Dept. of Mechanical and Industrial Engineering, Univ. of Illinois at Urbana–Champaign, Urbana, IL, 1997.

[18]Vollan, A., and Alati, L., "A New Optical Pressure Measurement System (OPMS)," 14th ICIASF Congress, Rockville, MD, Inst. of Electrical and Electronics Engineers, 91CH3028-8, New York, 1991.